buildings

Article

Experimental Study on Axial Compressive Performance of Light-Steel Skeleton–Cement–Fly Ash Foam Wallboard

Chengcong Liu [1,2], Yu Bai [1,2,*], Xinli Jiang [1,2] and Hexian Su [1,2]

1 Faculty of Civil Engineering and Architecture, Kunming University of Science and Technology, Kunming 650500, China; lcc13580649687@163.com (C.L.); lcc13580649688@163.com (X.J.)
2 Earthquake Engineering Researching Center of Yunnan, Kunming 650500, China
* Correspondence: baiyu@kust.edu.cn

Abstract: Foamed cement fly ash is a new type of lightweight construction material that can be combined with a light steel frame to form light-steel skeleton–cement–fly ash foam wallboard (LSSCFAFW). The research on the axial compressive performance of light steel and light concrete composite wallboard is relatively limited. Four pieces of LSSCFAFWs were manufactured, and the impact of stand column quantity and various filler parameters on the LSSCFAFW was investigated. The failure mode of the wallboard and the influence of different parameter variables on its axial compressive performance were obtained through experiments. Moreover, the test results indicated essentially the same damage patterns in terms of stand-column buckling, filler crushing, and self-tapping screw failure. The addition of polypropylene fiber to this wallboard can prevent filler from falling off. The axial compressive performance of the LSSCFAFW demonstrates a direct proportion with the number of columns and cement content, improving as the number of stand columns and the cement content increase. However, the addition of polypropylene fiber to the filler has a minimal effect on the axial compressive performance of this wallboard. Compared to the control group, increasing the number of stand columns, adding 0.4% polypropylene fibers, and increasing the cement dosage to 50% improved the ultimate bearing capacity of the wallboards by 12%, 8%, and 56% respectively. The result of this study can provide references for the research and application of light steel frame to form LSSCFAFW.

Keywords: composite wallboard; cement fly ash foam wallboard; polypropylene fiber; axial performance test; vertical bearing capacity

check for updates

Citation: Liu, C.; Bai, Y.; Jiang, X.; Su, H. Experimental Study on Axial Compressive Performance of Light-Steel Skeleton–Cement–Fly Ash Foam Wallboard. *Buildings* **2023**, *13*, 1928. https://doi.org/10.3390/buildings13081928

Academic Editor: Enrico Tubaldi

Received: 25 June 2023
Revised: 21 July 2023
Accepted: 27 July 2023
Published: 28 July 2023

1. Introduction

China's rural population is substantial, and as a result, the quantity of rural housing construction is steadily increasing. Rural housing constitutes a significant portion of the overall building stock. However, traditional rural housing suffers from poor quality and low load-bearing capacity, exacerbating issues of resource waste and environmental pollution. To tackle these pressing problems and promote the adoption of green and low-carbon prefabricated buildings in rural low-rise housing, the light steel and light concrete structural system was introduced during the 11th Five-Year Plan [1]. This system has gained significant attention and achieved a remarkable combination of prefabricated construction and cast-in-place construction in recent years due to its advantages, such as a simple construction process, affordability, excellent sound and heat insulation properties, high load-bearing capacity, etc. [2–5]; it has garnered considerable attention as a structural system in recent years.

Scholars in this field have conducted extensive studies on light-steel skeleton composite wallboards. Hegyi P. and Dunai L. [6] conducted vertical axial compressive tests on steel skeletons without polystyrene aggregate concrete (PAC) filling and cold-formed thin-walled composite wallboards with polystyrene aggregate concrete PAC filling. The results demonstrated that PAC effectively prevented steel skeleton buckling and enhanced joint load-bearing capacity, leading to a significant increase in the walls' overall bearing capacity. Dias Y. et al. [7] conducted vertical axial compressive tests on web-stiffened wall columns combined with gypsum board wallboards, revealing that web-stiffened C-sections as wall columns exhibit superior compressive load-bearing capacity compared to normal C-sections as wall columns. In a separate experimental study on cold-formed steel composite wallboards filled with gypsum-based composites, Chen J.W. et al. [8] analyzed the failure mode, axial compressive stiffness, and vertical bearing capacity of unfilled and filled wall specimens. Zhang Z.G. et al. [9] examined the impact of different wallboard materials on the axial compressive performance of light-steel composite wallboards. They found that composite wallboards clad with oriented strand board in the same stand-column cross-sectional form exhibited increased load-bearing capacity compared to walls clad with gypsum board. Vieira L., Jr. [10] and Fratamico, D.C. [11] demonstrated that cladding wallboards effectively limited overall buckling and suppressed local buckling of cold-forming sectional steel columns. Lastly, Ye, J. et al. [12] demonstrated that cladding wallboards can enhance the ultimate bearing capacity of composite wallboards by 20 to 27%.

Previous research has primarily focused on the axial compressive performance of light-steel skeleton composite wallboards using concrete as the filler material. However, there is a relative lack of research on the use of foaming building materials as fillers in light-steel skeleton composite wallboards. Furthermore, the existing research on the axial compressive performance of light steel and light concrete composite wallboards is insufficient, and there is a lack of experimental data to support the vertical load capacity and theoretical design of these wallboards. To address these gaps, this paper presents the design of a prefabricated LSSCFAFW (refer to Figure 1c). The main materials used in this wallboard are cold-formed thin-walled steel and foamed cement–fly ash. After assembling the light-steel skeleton, the cavity is filled with foamed cement–fly ash. Additionally, the wallboard utilizes a low-carbon and environmentally friendly fly ash construction material as its primary component. It exhibits lightweight characteristics, a high bearing capacity, ease of construction, sound and heat insulation, and environmental protection properties. The study aims to investigate the influence of various factors, including the number of stand columns, polypropylene fiber, and the cement content used on the axial compressive performance of the LFFCFAFW, four groups of LFFCFAFWs with different construction and materials were designed for vertical bearing capacity exploration. Furthermore, by studying the axial compressive performance test, the vertical bearing performance of this wallboard can be studied, which can give a complete response to the transmitted vertical load from the superstructure. This analysis helps identify the key factors and their failure modes affecting the mechanical performance of this wallboard, offering a theoretical foundation and technical support for their design and application promotion of this wallboard, and fills the knowledge gap regarding light steel and light concrete composite walls. Additionally, the research findings presented in this paper can serve as a valuable reference for other light steel and light concrete composite wall panels.

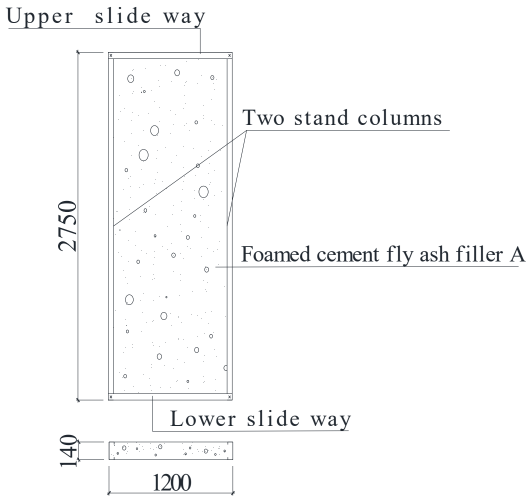

(**a**) Specimen YBV-1

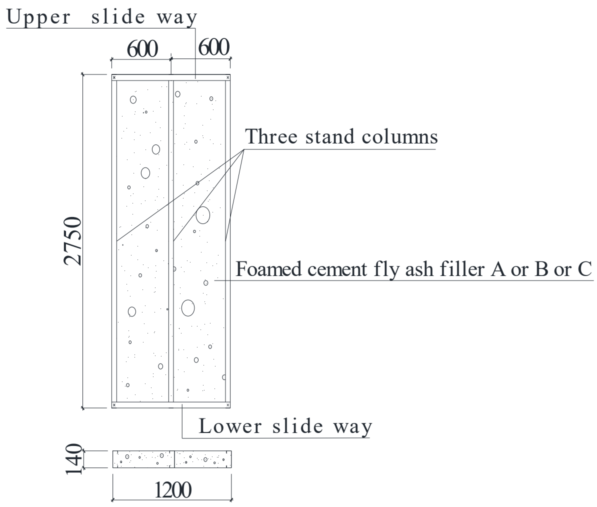

(**b**) Specimen YBV-2, YBV-3, and YBV-4

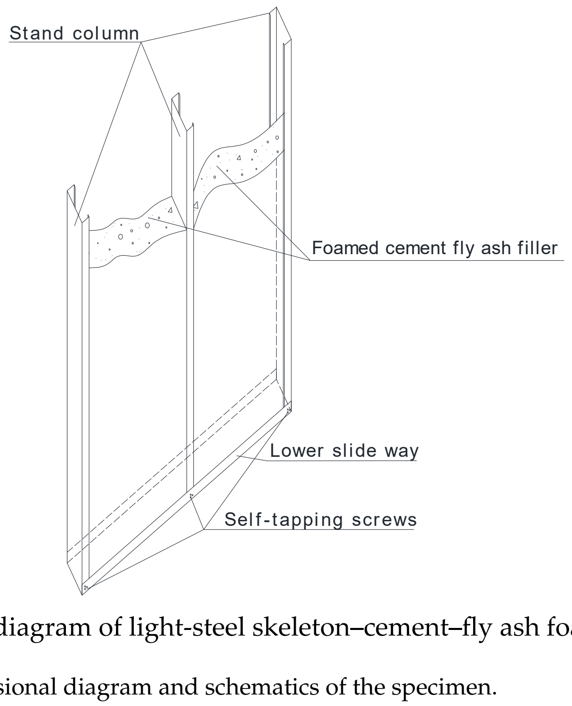

(**c**) Schematic diagram of light-steel skeleton–cement–fly ash foam wall panel

Figure 1. Dimensional diagram and schematics of the specimen.

2. Experimental Program

2.1. Material Characteristics

The foam cement–fly ash filler used in the study was categorized into three types: filler A, filler B, and filler C. Filler A consisted of 30% cement, 70% fly ash, and 0.5% foaming agent. Filler B had a composition of 30% cement, 70% fly ash, 0.4% polypropylene fiber, and 0.5% foaming agent. Filler C contained 50% cement, 50% fly ash, and 0.5% foaming agent. The foam and the fiber were proportioned by weight. The cement used was commercially available P.O42.5 ordinary silicate cement; the fly ash used was commercially available Class III fly ash; the polypropylene fiber used was commercially available 6 mm polypropylene fiber. Additionally, the foaming agent employed in the study was developed by the Environmental Materials Laboratory at the School of Chemistry and Engineering, Kunming University of Science and Technology. To assess the material performance of the foam cement–fly ash filler, it was subjected to tests in accordance with the JG/T 266-2011 Foamed Concrete standard [13]. A total of 3 cubes (100 mm × 100 mm × 100 mm) and 3 prisms (100 mm × 100 mm × 300 mm) were fabricated using the same batch of foamed cement–fly ash filler as the test specimen, and the results were averaged. The test results are listed in Table 1. The standard deviations of the filler′s density, compressive strength, and elastic modulus are 41.55, 1.08, and 1391.38, respectively.

Table 1. Characteristics of foamed cement fly ash materials.

Filler Number	Dry Density/kg·m^{-3}	Compressive Strength/MPa	Elastic Modulus/MPa
A	867.50	4.27	3587
B	826.20	4.60	3831
C	927.40	6.72	6653

The grade 550 C aluminized zinc-coated thin-walled steel plate utilized in the experiment underwent tensile testing in accordance with the GB/T228.1-2010 Metallic Materials—Tensile Testing—Part I: Method of Test at Room Temperature standard [14]. To ensure consistency, the same batch of steel used in the composite wallboard was selected for processing. Three samples were tested, and the test results were averaged. The test results for the steel plate are presented in Table 2. The standard deviations of yield strength, tensile strength, elastic modulus, elongation rate after fracture, and Poisson's ratio for the steel are 13.07, 15.09, 4472.13, 0.02, and 0.01, respectively.

Table 2. Characteristics of steel materials.

Steel Plate Thickness/mm	Yield Strength/MPa	Tensile Strength/MPa	Elastic Modulus/MPa	Elongation Rate after Fracture/%	Poisson's Ratio
1.00	728.60	738.80	2.07×10^5	11.00	0.24

2.2. Experimental Design

The test was conducted following the guidelines outlined in JGJ 383-2016 Technical Specification of Lightweight Steel and Lightweight Concrete Structures [15] and JGJ 227-2011 Technical Specification for Low-rise Cold-formed Thin-wall Steel Buildings [16]. According to JGJ 383-2016 and JGJ 227-2011, the spacing between light steel columns should not exceed 600 mm. Therefore, the stand column spacing in this study was set at 600 mm. These codes specify that for seismic fortification intensities of 6 and 8, the maximum height of the houses is 20 m and 10 m, respectively and the maximum number of floors is 6 and 3, respectively. This translates to a floor height of approximately 3.33 m, considering a standard beam height of 600 mm for rural housing. Consequently, the wall boards designed in this paper had a height of 2750 mm. Furthermore, the regulations stipulate that the thickness of the light steel and light concrete shear wall should be at least

140 mm. Hence, the wall panel thickness in this study was set at 140 mm. Four full-size LSSCFAFWs were designed and constructed for the experiment. The dimensions of the wallboards were 1.2 m × 0.14 m × 2.75 m (width, thickness, and height). Specimen YBV-1 had a stand-column spacing of 1.2 m, while specimens YBV-2, YBV-3, and YBV-4 had a stand-column spacing of 0.6 m. Figure 1 illustrates the schematic depiction of the dimensions of the four wallboards, and Table 3 provides the parameters of the specimens. To ensure stability, the light-steel skeleton of each specimen was secured using stand columns, slide ways, and steel tie strips. The connection between the stand column and slide way was achieved using self-tapping screws ST4.2. The slide way and column were constructed using C140 × 40 × 10 × 1 cold-formed thin-walled C-section members. Additionally, the four specimens were made from galvanized thin-walled steel sheets with a thickness of 1 mm and a steel strength grade of 550 MPa.

Table 3. Specimen parameters.

Specimen Number	Number of Stand Columns/Piece	Filler Type
YBV-1	2	A
YBV-2	3	A
YBV-3	3	B
YBV-4	3	C

To produce wall specimens, first, assemble the light-steel skeleton, and then pour the foam cement–fly ash filler into the light steel skeleton (pouring horizontally). The pouring process should be conducted continuously six times, with each pouring producing a 100 mm cube specimen and a 100 mm × 100 mm × 300 mm prism specimen of the foam cement–fly ash filler.

2.3. Sensor Placement

The test primarily measured the vertical load and vertical displacement of the specimen, the vertical strain distribution at the bottom of the light-steel skeleton stand column, the vertical strain distribution at the bottom of the cement fly ash foam wallboard, and the out-of-plane displacement at the middle of the wallboard. The vertical load and vertical displacement were obtained from the pressure testing machine, while the strain was obtained from the strain gauges. The out-of-plane displacement of the wallboard was measured by the top rod displacement meter (designated as D1). For the wallboard with two stand columns, the strain gauges S1 to S4 measured the vertical strain of the light-steel skeleton, and the strain gauges F1, F3, and F5 measured the vertical strain at the bottom of the cement fly ash foam wallboard. Additionally, the strain gauges F2, F4, and F6 measured the transverse strain at the bottom of the foamed cement wallboard. For the wall panels with three stand columns, the strain gauges S1 to S6 measured the vertical strain of the light-steel skeleton, and the strain gauges F1 to F4 measured the vertical strain at the bottom of the cement fly ash foam wallboard. The arrangement of displacement meters and strain gauges is illustrated in Figure 2.

2.4. Experiment Setup and Loading Program

The axial compressive performance test was conducted using an electro-hydraulic servo pressure testing machine, and the uniform loading scheme was utilized. Align the test specimen geometrically with the testing machine, ensuring that the top of the test specimen comes into direct contact with the pressure plate of the testing machine. Secure the bottom of the specimen using a U-shaped steel plate to ensure uniform contact between the test specimen and the testing machine. The vertical load is evenly transmitted through the pressure plate of the testing machine to the top of the test specimen, resulting in a simultaneous compression of the fill material and the column. Before the actual test loading, a vertical load of 5 kN was applied to ensure the proper functioning of the inspection and testing system. During the formal loading phase, the specimen was subjected to a uniform rate of 0.5 kN per second until failure occurred. The experimental loading diagram can be seen in Figure 3.

(**a**) Two stand columns

(**b**) Three stand columns

Figure 2. Strain gauge and displacement arrangement of the specimen.

Figure 3. Test loading diagram.

3. Specimen Failure Phenomenon and Characteristics

3.1. Specimen YBV-1

The loading of the specimen initially showed no obvious signs of failure. Moreover, at a vertical load of 20 kN, a loud sound was heard. As the load increased to 210 kN, the filler material at the top of the specimen started to crush and slag fell off (Figure 4a). When the load reached 410 kN, the specimen completely lost its load-bearing capacity. The top of the filler material was instantly crushed (Figure 4c), causing the connection site between the upper slide way and the stand column to be crushed. The stand column itself bulged, crumbled, and detached from the filler (Figure 4b).

3.2. Specimen YBV-2

At the early stage of loading, there was no obvious change in the specimen; at approximately 460 kN, the filler at the top back of the specimen started to fall off (Figure 5a). Simultaneously, a vertical crack extended downward from the top of the specimen (Figure 5b). On one side of the specimen, the stand column became separated from the filler block (Figure 5c), and the self-tapping screw connection between the upper slide way and the side stand column failed (Figure 5d). These events occurred when the specimen reached its maximum load-bearing capacity, resulting in failure.

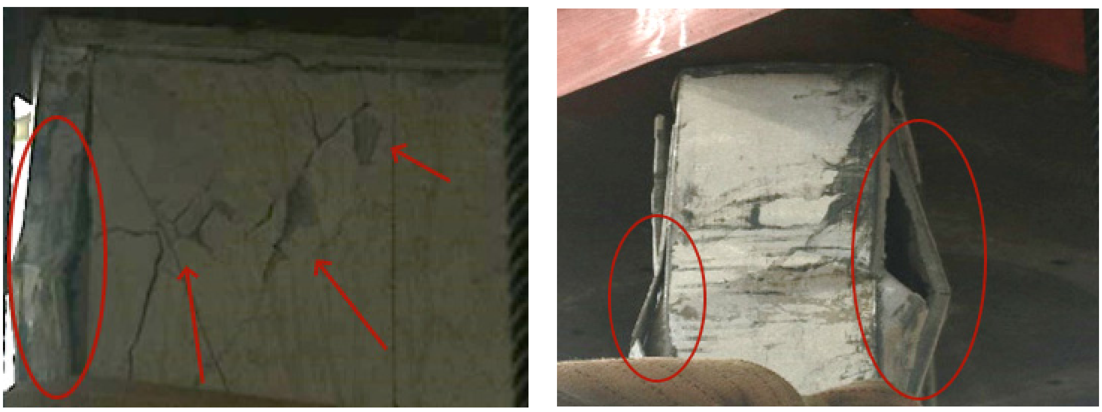

(**a**) Cement board crushing (**b**) Steel buckling and crumbling

Figure 4. *Cont.*

(**c**) Filler crushing and falling off

Figure 4. Failure characteristics of specimen YBV-1 (Red circles and arrows are prominent phenomena in the figure commented).

(**a**) Top filler falling off

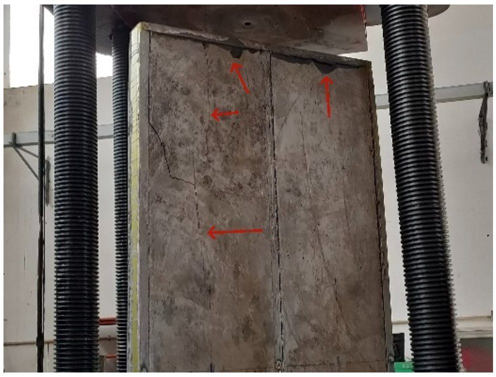

(**b**) Vertical cracks

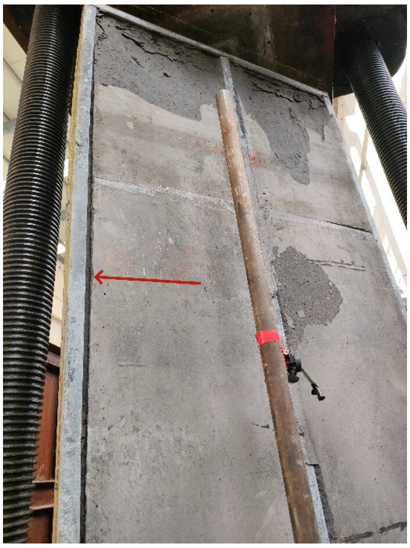

(**c**) Separation of stand column and filler

(**d**) Self-tapping screw failure

Figure 5. Failure characteristics of specimen YBV-2 (Red circles and arrows are prominent phenomena in the figure commented).

3.3. Specimen YBV-3

In the early stage of loading, no apparent failure was observed in the specimen, and the strain on the wall continued to increase. At approximately 280 kN of load, a distinct "pop" sound was heard, and the cement board separated from the web of the middle stand column (Figure 6a). As the load reached about 496 kN, the upper right and lower left fillers of the specimen crushed and failed, while the remaining fillers appeared intact (Figure 6b). Furthermore, when the vertical load approached its peak, the middle stand and side columns exhibited buckling deformation (Figure 6c,d). The warping flange of the upper slide way and the self-tapping screws failure were observed (Figure 6d). Ultimately, the specimen lost its load-bearing capacity.

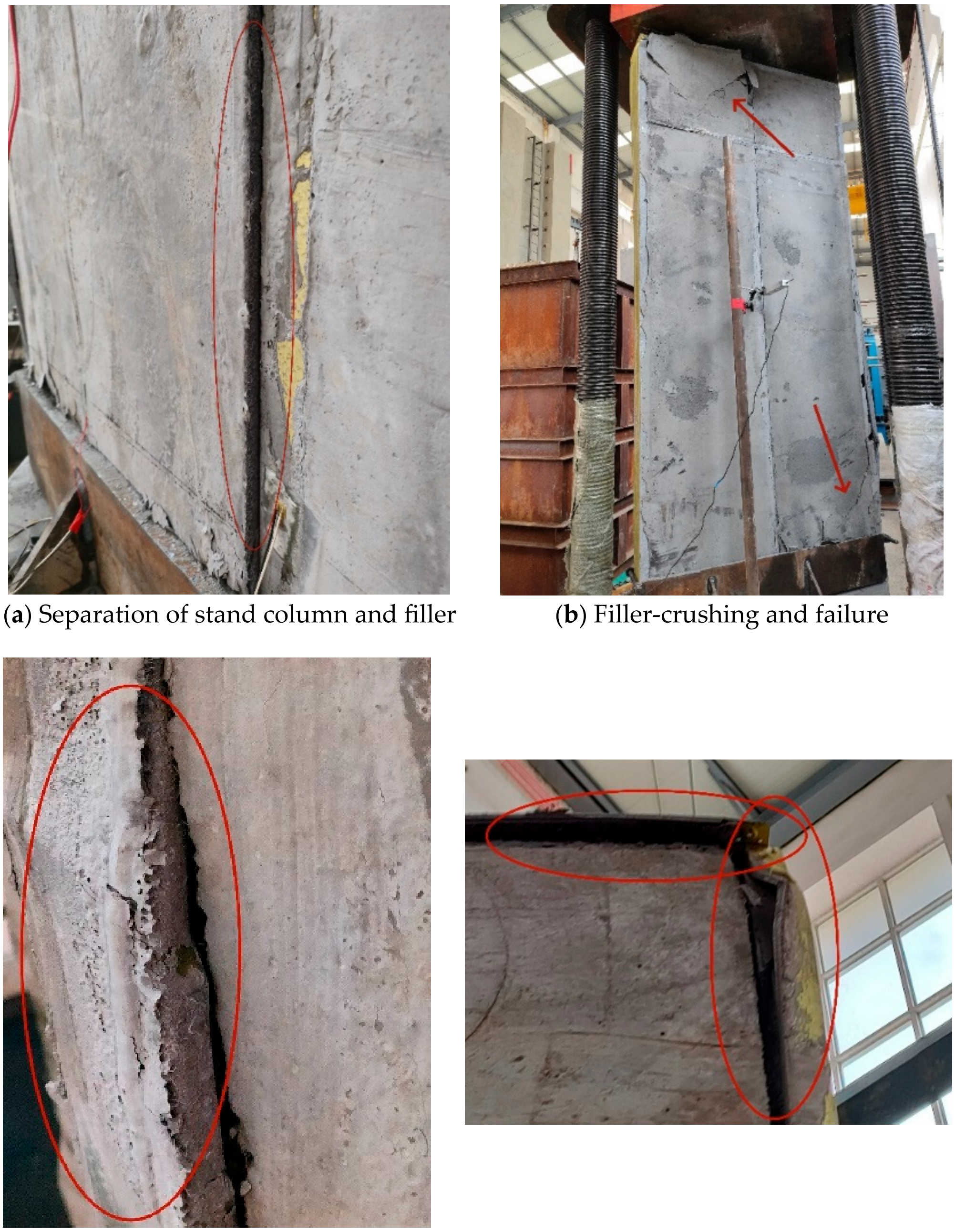

(**a**) Separation of stand column and filler
(**b**) Filler-crushing and failure
(**c**) Stand-column buckling and deformation
(**d**) Slide way warping and self-tapping screw failure

Figure 6. Failure characteristics of specimen YBV-3 (Red circles and arrows are prominent phenomena in the figure commented).

3.4. Specimen YBV-4

The specimen did not show any noticeable changes before the load reached 600 kN. Moreover, at a load of 600 kN, the specimen produced a "pop" sound, and two vertical cracks emerged in the middle of the foam cement board. As the load increased, these propagated from the middle of the wallboard towards the top and bottom (Figure 7a). This behavior is consistent with the test of Prabha P. [17], which observed the phenomenon of vertical cracking and failure of the wallboard. At a load of 722 kN, a large piece of filler at the top of the specimen detached from the outside to the inside (Figure 7b). The increased load was transferred to the stand column, causing warping and distortion of the flange of the side column (Figure 7c). These visible signs indicated the specimen's clear failure, and it reached its ultimate bearing capacity.

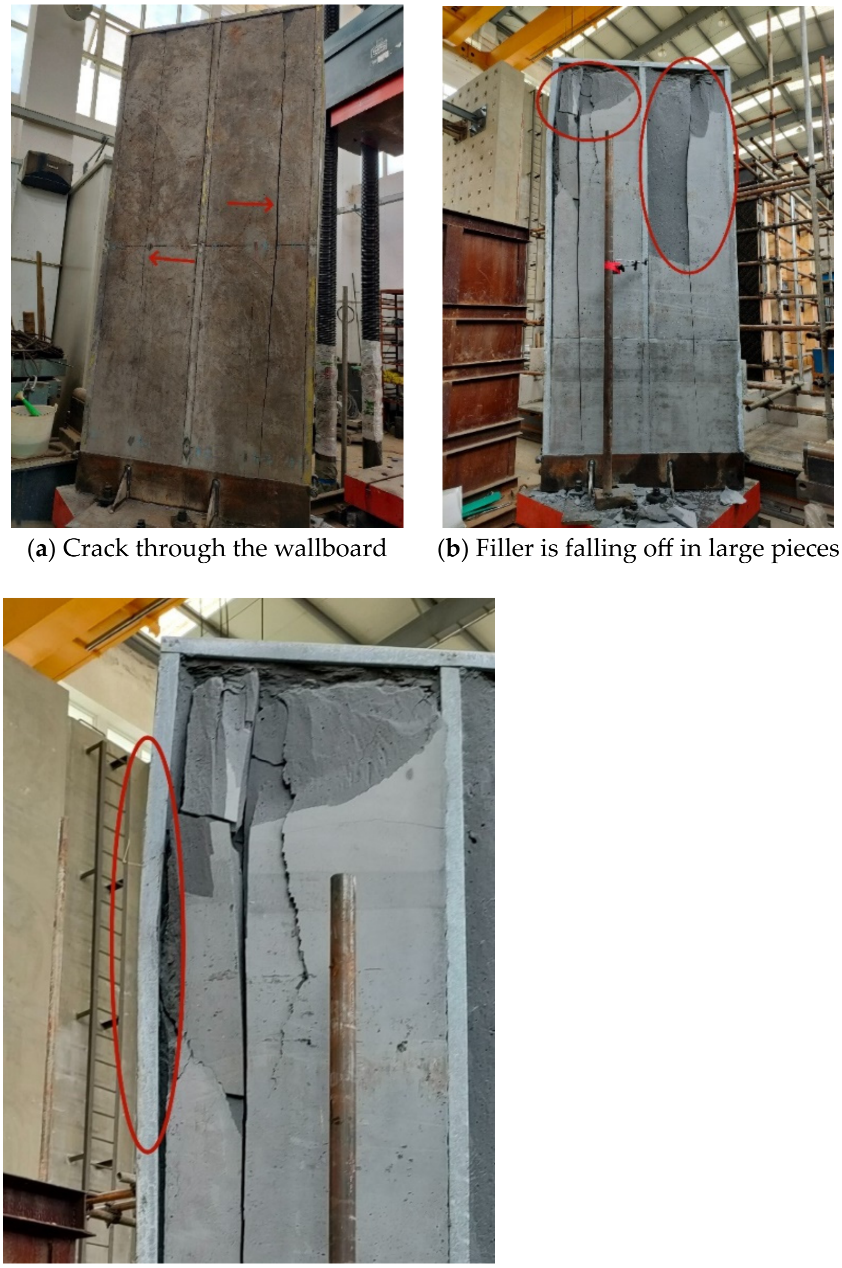

(**a**) Crack through the wallboard (**b**) Filler is falling off in large pieces

(**c**) Side column buckling deformation

Figure 7. Failure characteristics of specimen YBV-4 (Red circles and arrows are prominent phenomena in the figure commented).

4. Experimental Results and Analysis

The load–displacement curves were obtained from test results, comparing the vertical load–displacement relationships of the LSSCFAFW specimens with varying numbers of stand columns, different cement content, and mixed with polypropylene fiber. Figure 8 illustrates these comparisons.

The ultimate bearing capacity and ultimate displacement values of each specimen were determined based on their respective load–displacement curves. An analysis was conducted to examine the influence of factors such as the number of stand columns, cement content, and the addition of fiber on the ultimate bearing capacity and ultimate displacement of each specimen were analyzed. The findings of this analysis are presented in Table 4. The results were compared by comparing YBV-3 and YBV-4 with YBV-2, and YBV-2 with YBV-1. The comparative results can be found in Table 4.

Table 4. Table of ultimate bearing capacity and ultimate displacement of the specimen.

Specimen Number	Ultimate Bearing Capacity/kN	The Percentage Difference	Ultimate Displacement/mm	The Percentage Difference
YBV-1	412		5.01	
YBV-2	460	+12%	5.09	+2%
YBV-3	496	+8%	6.07	+19%
YBV-4	720	+56%	5.25	+3%

4.1. Effect of the Number of Columns on the Vertical Bearing Capacity of Wallboards

Observations from Figures 8 and 9 and Table 4 reveal certain patterns in the load–displacement and load–strain curves initially, during the compression phase, both the two-stand column and three-stand column wallboards exhibited a prolonged elastic phase (before the 282 kN of YBV-1 and the 339 kN of YBV-2, refer to the arrow in Figure 8a), indicating a positive synergistic force effect between the fillers and the columns. Subsequently, in the plastic phase, cracks and fragmentation occurred in the top filler, causing the bottom filler to protrude in terms of strain value (refer to the arrow in Figure 9a,c). At this stage, the primary bearing role gradually shifted to the columns. As the load approached its peak (the 412 kN of YBV-1 and the 460 kN of YBV-2), the stand columns experienced buckling (as shown in Figure 4b), and there was significant crushing and falling off of the filler (as shown in Figures 4c and 5a). Consequently, the strain of the filler and steel exhibited a sharp decline (the circle in Figure 9), resulting in a step-down in the bearing capacity of the wallboard and ultimately leading to specimen failure, which aligns with the observed failure characteristics. Furthermore, Figure 9b,d demonstrates that the strains at the bottom of the side columns in the three-stand column wallboard ranged from -500 $\mu\varepsilon$ to -600 $\mu\varepsilon$, whereas in the two-stand column wallboard, these strains ranged from -700 $\mu\varepsilon$ to -850 $\mu\varepsilon$. Additionally, the strains in the middle stand columns reached as high as between -1500 $\mu\varepsilon$ and -1700 $\mu\varepsilon$. These differences indicate that the separation of the filler from the stand column, along with the occurrence of crushing and falling off of the filler at the top of the wallboard, transpired during the compression process of the three-stand column wallboards. Moreover, as the load increased, the force mechanism of the wallboard transformed. The strain value of the middle stand column surpassed that of the side columns (as evident in Figure 9d for strain gauges S2 and S5), signifying that the stand column assumed the primary compression-bearing role, effectively leveraging its load-bearing capacity during the compression process and thereby improving the vertical bearing capacity of the wall.

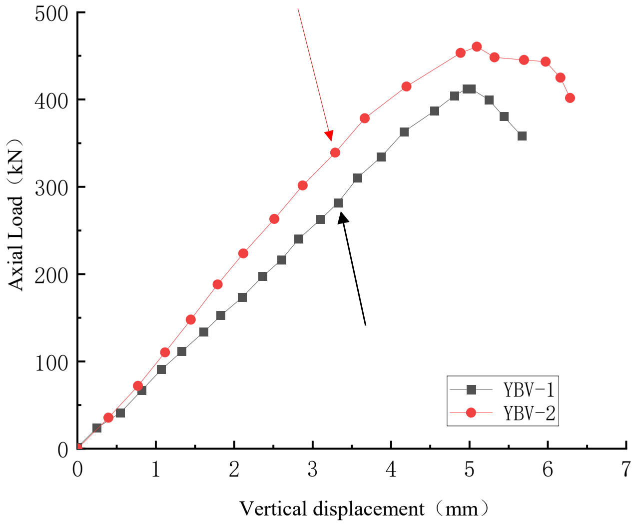

(**a**) Comparison of the number of stand columns

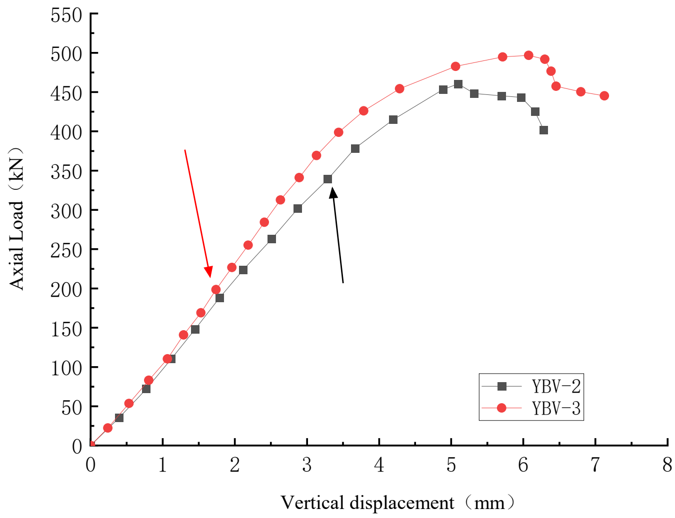

(**b**) Comparison of adding fiber

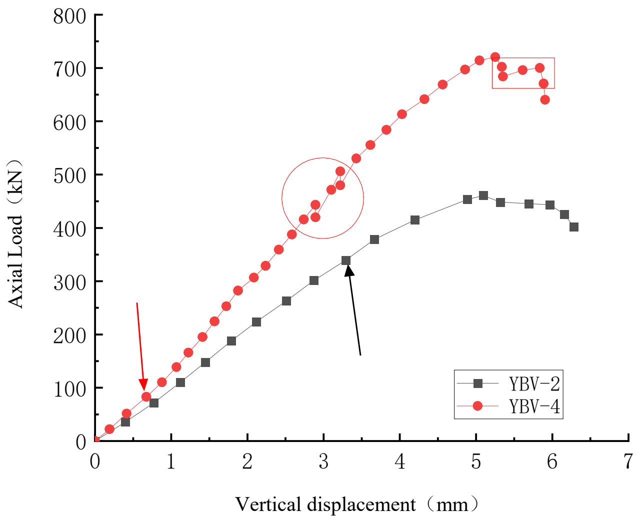

(**c**) Comparison of the cement content

Figure 8. Load–displacement curves (Red circles and arrows are prominent phenomena in the figure commented).

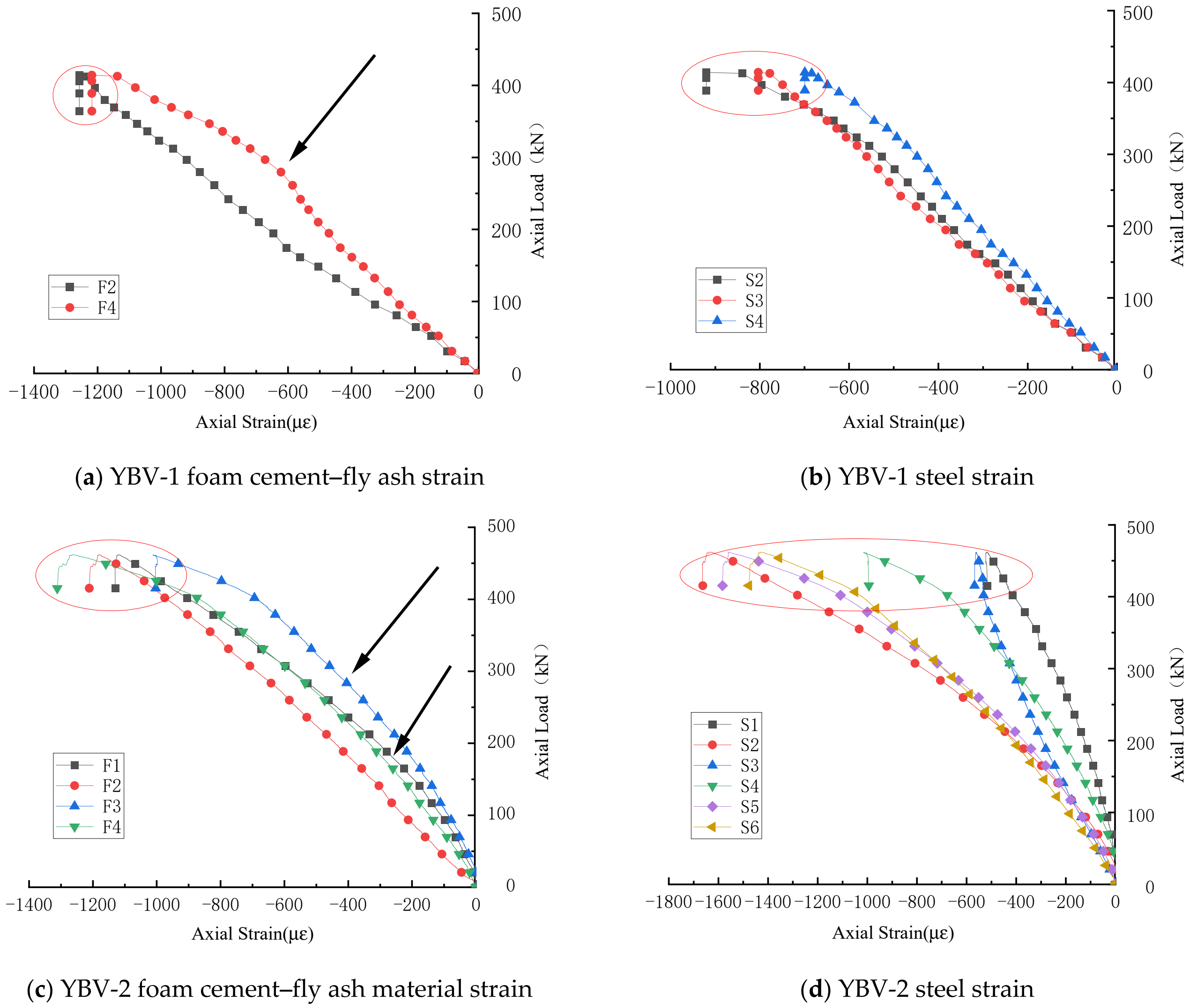

Figure 9. Load–strain curve (Red circles and arrows are prominent phenomena in the figure commented).

In comparison to the two-column wall panels, the three-stand column wallboards exhibited higher stiffness (103.08) during loading and achieved an ultimate bearing capacity approximately 12% higher than the two-stand column wallboard. This disparity can be attributed to the presence of the filler, which restrained the buckling of the middle stand column and allowed it to share a portion of the vertical load. Consequently, the vertical ultimate bearing capacity and initial stiffness of the wallboards increased, leading to enhanced safety and stability.

4.2. Effect of Polypropylene Fiber on the Vertical Bearing Capacity of Wallboard

From Figures 8b and 10, compared to the wallboard without fiber (YBV-2), the wallboard with fiber (YBV-3) exhibited elastic properties only during the initial stage of compression. This is due to the addition of fibers, which enhances the bonding force between the fillers [18] and reduces the recovery deformation capability of the fillers. As the load increased, the walls entered the plastic stage (339 kN for YBV-2 and 198 kN for YBV-3, refer to the arrow in Figure 8b), and the displacement and strain continued to increase gradually, albeit with a decreasing slope in the curve. Notably, the inclusion of polypropylene fiber in the filler enhanced its elastic modulus, ductility deformation capacity, and crack resistance. Consequently, specimen YBV-3 demonstrated a more prolonged plastic deformation phase before reaching the ultimate state. This leads to an improved load-bearing capacity of the filler and a more favorable trend in its strain values (refer to Figure 10). On the other hand, specimen YBV-2 exhibited relatively weaker plastic behavior (as seen in Figure 8b), coupled with the crushing failure of a large filler area and local buckling of its stand column (as depicted in Figure 6). This resulted in a sudden increase in the strain values of the filler and steel in the fiber wallboard (refer to the arrow in Figure 10, strain gauges F1, F4, and S5). With continued loading, the bearing capacity of this wallboard reached its limit (496 kN for YBV-3), causing the load–displacement and load–strain curves to drop sharply (the circle in Figure 10), ultimately leading to the failure of the wallboard.

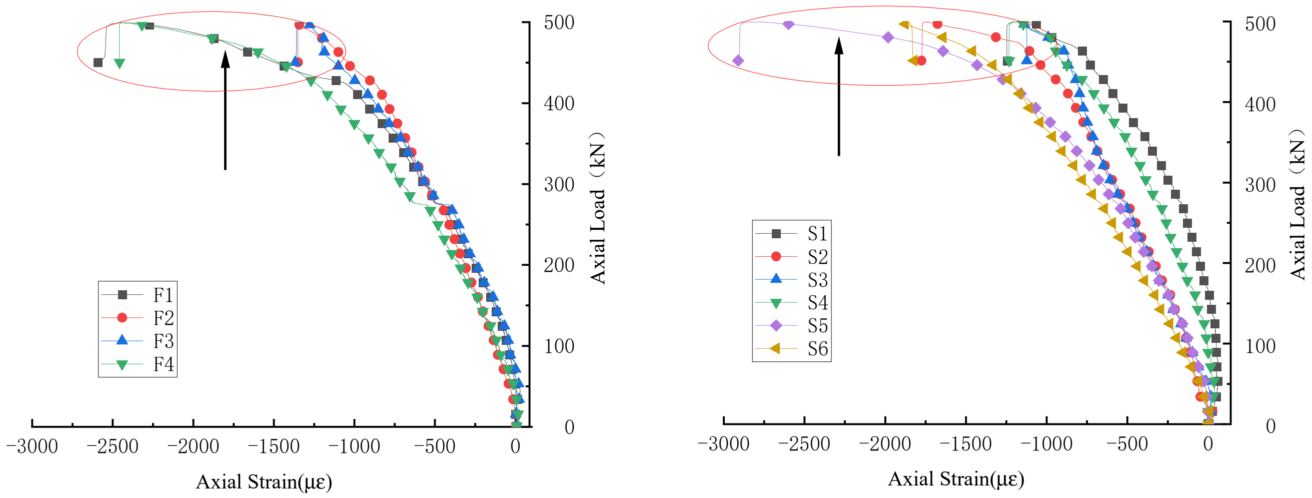

(**a**) YBV-3 Foam cement–fly ash strain (**b**) YBV-3 Steel strain

Figure 10. Load–strain curve (Red circles and arrows are prominent phenomena in the figure commented).

When comparing the wallboards with and without fibers, it is evident that the fiber wallboards exhibited slightly higher stiffness (114.07), ultimate bearing capacity, and ultimate displacement compared to the fiberless wallboards. Specifically, the ultimate bearing capacity and ultimate displacement of the fiber wallboards were approximately 8% and 19% higher, respectively, than that of the fiberless wallboards. This improvement can be attributed to the addition of 0.4% polypropylene fiber, which enhances the compressive strength of the filler, elastic modulus, and bonding force between its fillers [18,19]. As a result, the overall deformation capacity and bearing capacity of the wallboards were enhanced. Furthermore, by comparing the changes in strain values between the fiberless and fiber wallboards (as shown in Figure 9c,d and Figure 10), it can be observed that the strain values of the foam cement–fly ash filler and steel strains in the fiber wallboards primarily ranged between −1300 με and −2600 με and −1100 με and −1900 με, respectively. In contrast, the strain values of the cement–fly ash foam filler and steel strains in the fiberless wallboards mainly ranged between −1000 με and −1300 με and −500 με and −1700 με, respectively. The strain values in the fiber wallboards were higher than those in the fiberless wallboards, indicating that the addition of polypropylene fiber increased the elastic modulus and bonding force of the filler. This allowed the wallboards to withstand higher vertical loads, leading to increased wall deformation and a corresponding rise in the strain values of the filler and steel.

4.3. Effect of the Cement–Fly Ash Foam's Cement Content on the Vertical Bearing Capacity of Wallboard

From Figure 8c, it is evident that the slope of specimen YBV-4 was significantly larger than that of specimen YBV-2 throughout the compression process. Unlike the wall panel with 30%, specimen YBV-4 remained in the elastic stage until the load reached 85 kN (refer to the arrow in Figure 8c). Subsequently, during the plastic stage of specimen YBV-4, the load increase led to the gradual separation between the filler and stand column, as well as the development of cracks within the filler. The load–displacement curve of this wallboard exhibited two sudden drops (as shown in the circle in Figure 8c) when the load reached 443 kN and 506 kN. Notably, specimen YBV-4 exhibited a sudden increase (with a load of 684 kN, as shown by the rectangle in Figure 8c) in the bearing capacity during the yielding stage. This was attributed to excessive deformation causing a significant gap between the filler and the stand column, resulting in the sudden detachment of the top of the filler. Consequently, the bearing capacity of the wallboard decreased, accompanied by a distinct and sudden change in steel strain (as observed in F3, F4, S1–S4, and S6). Continuing the loading process, the filler and stand column came into contact again, leading the bearing to another sudden increase in bearing capacity. This behavior aligns with previous studies [20] that observed similar changes in load-bearing capacity. These findings indicate a strong joint force effect between the filler and stand column in specimen YBV-4. Importantly, the self-tapping screws remained intact and did not fail when the specimen exhibited obvious failure characteristics (refer to Figure 7). This suggests that the self-tapping screws effectively facilitated the connection between the foam cement–fly ash filler and the stand column, demonstrating their favorable role in maintaining structural integrity.

When comparing the load-bearing capacity of wallboards with different cement contents, it is evident that the increase in cement content had a significant impact on their bearing capacity and initial stiffness (the stiffness of YBV-2 was 103.08, while that of YBV-4 was 124.06). The wallboards with 50% cement content exhibited much greater stiffness than those with 30% cement content, and their ultimate bearing capacity was approximately 56% higher compared to the 30% cement content wallboards. Furthermore, by examining Figures 9c and 11a, it was observed that the strain values of the filler in the 50% cement content wallboards primarily ranged between -1000 με and -1400 με, while for the 30% cement content wallboards, the strain values ranged between -1000 με and -1300 με. Although the strain values fluctuated similarly in both types of wallboards, the ultimate bearing capacity of the 50% cement-content wallboards was 1.56 times higher than that of the 30% cement-content wallboards. There are two main reasons for this difference. Firstly, increasing the cement content enhanced the compressive strength and elastic modulus of the foam cement–fly ash, thereby strengthening the foam cement–fly ash filler and improving the bonding stress between the foam cement–fly ash and the self-tapping screws. Secondly, increasing the cement content enhanced the buckling effect of the filler in suppressing the stand column, thus improving the joint bearing effect of the filler and the light-steel skeleton and effectively improving the vertical bearing capacity of the specimen. Consequently, the vertical bearing capacity of the specimen was significantly improved. It is worth noting that when compared to previous studies on the axial compressive performance of light-steel composite wallboards [21–23], these two types of LSSCFAFWs demonstrated an increase in the ultimate bearing capacity of approximately 1.2–2 times. Additionally, by reducing the fly ash admixture, the ratio of fly ash to cement can be optimized, enabling the active ingredients in fly ash to effectively bind with cement [24], thereby enhancing the bearing capacity of the wallboard.

According to relevant researchers, the amount of fly ash should not exceed 45% [25]. It is noted that an increase in fly ash content leads to a reduction in the strength of foam concrete [26]. However, a high fly ash content can also fulfil the requirements of lightweight and high-strength foam concrete [27], and the fly ash content in YBV-4 is as high as 50%, which has good bearing capacity and also meets the requirements of light steel and light concrete structures. This achievement holds significant importance for resource recycling and the realization of sustainable development.

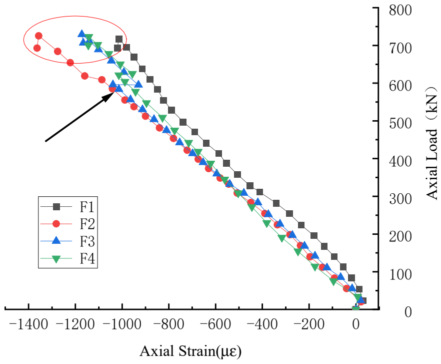

(**a**) YBV-4 Foam cement–fly ash strain

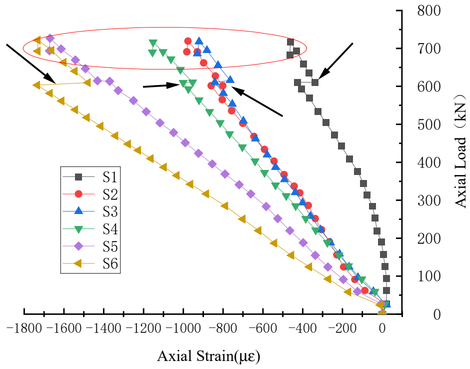

(**b**) YBV-4 Steel strain

Figure 11. Load–strain curve (Red circles and arrows are prominent phenomena in the figure commented).

5. Conclusions

Based on the conducted axial compressive performance tests on the LSSCFAFWs, the following conclusions were drawn:

(1) The failure modes observed in the four tested wallboards were primarily column buckling and foam cement–fly ash filler crushing. Enhancing the axial compressive performance of the wallboards can be achieved through various means, such as increasing the number of stand columns, increasing the cement content, and incorporating polypropylene fibers.

(2) Compared with the two-stand column LSSCFAFW, the vertical bearing capacity of the three-stand column composite wall panel is increased by approximately 12%. Additionally, by increasing the number of stand columns, the vertical bearing capacity and the safety stability of the LSSCFAFW are also improved accordingly.

(3) Adding 0.4% polypropylene fiber in the LSSCFAFW has little effect on the vertical bearing capacity of the wallboard, which is only increased by 7.8%. However, the mixing of polypropylene fiber increases the bonding force of the filler and improves the deformation capacity and crack resistance of the wallboard. This inhibits the falling of the filler and enhances the integrity of the wallboard. Therefore, polypropylene fiber can be mixed in the wall panel to improve the integrity of the wallboard.

(4) By increasing the cement content, the vertical bearing capacity of the LSSCFAFW can be effectively improved. This enhances the buckling and bending deformation resistance of the stand columns and strengthens the joint bearing effect of the filler, and the light-steel skeleton is enhanced. Compared with the composite wallboard, the vertical bearing capacity of the 50% cement content composite wallboard with 50% cement content is increased by approximately 56%. Furthermore, the elastic modulus of the foam cement–fly ash filler is doubled. This mitigates the negative impact of increased cost for the wallboard.

Author Contributions: Conceptualization, C.L. and Y.B.; data curation, C.L. and X.J.; methodology, C.L.; software, C.L. and X.J.; validation, Y.B. and H.S.; writing—original draft, C.L. and X.J.; writing—review and editing, Y.B. and H.S. All authors have read and agreed to the published version of the manuscript.

Funding: National Natural Science Foundation of China (51368027).

Institutional Review Board Statement: Not applicable.

Informed Consent Statement: Informed consent was obtained from all subjects involved in the study.

Data Availability Statement: Data will be made available on request.

Acknowledgments: Thanks to Zhiyun for providing the language polishing support for this research.

Conflicts of Interest: The authors declare no conflict of interest.

References

1. Huang, Q.; Li, D.B.; Wang, J.J.; Chen, C.A.; Zhang, M. Study on lightweight steel and lightweight concrete structures system. *J. Build. Struct.* **2016**, *37*, 1–9. [CrossRef]
2. Zhao, J.B.; Huang, S.; Fu, H.; Jiang, Y.; Chu, Y. Research on the application of light steel and lightweight concrete structures in rural housing. *Constr. Wall Innov. Build. Energy-Sav.* **2019**, *12*, 70–71. [CrossRef]
3. Liu, W.; Zhou, E.Z. Summary of the development of light steel light concrete structural system. *Sichuan Build. Mater.* **2019**, *45*, 87–88. [CrossRef]
4. Rybakov, V.; Seliverstov, A.; Raimova, I. Lightweight steel-concrete wall bearing structures under high-temperature exposure. In *AIP Conference Proceedings*; AIP Publishing: Melville, NY, USA, 2023; Volume 2612.
5. Zhang, J.; Zhao, F. Applications of Light Steel and Light Concrete Structure System in Island Building. *J. Coast. Res.* **2020**, *107*, 73–76. [CrossRef]
6. Hegyi, P.; Dunai, L. Experimental study on ultra-lightweight-concrete encased cold-formed steel structures Part I: Stability behaviour of elements subjected to bending. *Thin-Walled Struct.* **2016**, *101*, 75–84. [CrossRef]
7. Dias, Y.; Mahendran, M.; Poologanathan, K. Axial compression strength of gypsum plasterboard and steel sheathed web-stiffened stud walls. *Thin-Walled Struct.* **2019**, *134*, 203–219. [CrossRef]
8. Chen, J.W.; Fan, K.; Gao, L. Experimental study on axial compression performance of cold-formed steel framing walls with infilled gypsum based material. *Build. Sci.* **2018**, *34*, 48–53.
9. Zhang, Z.N.; He, G.W.; Wang, C.G.; Kong, D.; Nie, L.; Liu, G. Experimental study on axial compression behavior of cold—Formed thin—Walled steel stud walls with stiffened—Web. *J. Build. Struct.* **2021**, *42*, 103–109.
10. Vieira, L., Jr.; Shifferaw, Y.; Schafer, B.W. Experiments on sheathed cold-formed steel studs in compression. *J. Constr. Steel Res.* **2011**, *67*, 1554–1566. [CrossRef]
11. Fratamico, D.C.; Torabian, S.; Zhao, X.; Rasmussen, K.J.R.; Schafer, B.W. Experimental study on the composite action in sheathed and bare built-up cold-formed steel columns. *Thin-Walled Struct.* **2018**, *127*, 290–305. [CrossRef]
12. Ye, J.; Feng, R.; Chen, W.; Liu, W. Behavior of cold-formed steel wall stud with sheathing subjected to compression. *J. Constr. Steel Res.* **2016**, *116*, 79–91. [CrossRef]
13. *Foamed Concrete (JG/T 266–2011)*; China Industry Standard. Architecture & Industry Press of China: Beijing, China, 2011.
14. *GB/T 228.1-2010*; National Standard of the People's Republic of China. Metallic Materials—Tensile Testing—Part 1: Method of Test at Room Temperature. China Architecture & Building Press: Beijing, China, 2010.
15. *JGJ 383—2016*; Technical Specification of Lightweight Steel and Lightweight Concrete Structures. China Architecture & Building Press: Beijing, China, 2016.
16. *JGJ 227—2011*; Technical Specification for Low-Rise Cold-Formed Thin-Walled Steel Buildings. China Architecture & Building Press: Beijing, China, 2011.
17. Prabha, P.; Marimuthu, V.; Saravanan, M.; Palani, G.S.; Lakshmanan, N.; Senthil, R.A. Effect of confinement on steel-concrete composite light-weight load-bearing wall panels under compression. *J. Constr. Steel Res.* **2013**, *81*, 11–19. [CrossRef]
18. Wang, Z.Q.; Tan, K.F.; Xu, X.X. The Influence of Fiber on Properties of Foam Concrete. *J. Southwest Univ. Sci. Technol.* **2013**, *28*, 11–15.
19. Zhang, X.S.; Zhu, Y.F.; Huang, L.C. Effect of polypropylene fiber on mechanical properties of foamed concrete. *New Build. Mater.* **2019**, *46*, 140–142+147.
20. Zhang, X.H.; Zhang, E.Y.; Yu, H. Axial compression performance of coldformed thin-walled square steel stud-straw board composite wall. *Sci. Technol. Eng.* **2021**, *21*, 283–289.
21. Xu, Z.F.; Chen, Z.F.; Zhu, S.S.; Liu, J.; Yin, Z.Q. Study of lightweight steel high-strength foamed concrete shear wall covered with straw board subjected to axial loading. *Eng. Mech.* **2018**, *35*, 219–231.
22. Wu, H.; Chao, S.; Zhou, T.; Liu, Y. Cold-formed steel framing walls with infilled lightweight FGD gypsum Part II: Axial compression tests. *Thin-Walled Struct.* **2018**, *132*, 771–782. [CrossRef]
23. Xu, Z.; Chen, Z. Experimental investigation on cold-formed steel foamed concrete composite wall under compression. *Int. J. Civ. Environ. Eng.* **2017**, *11*, 1257–1263.
24. Xia, Q.; Ye, C.; Zhang, H.F. Study on foam concrete type light weight walling materials. *Concrete* **2010**, 127–128+132.
25. Qiu, J.F.; Luo, S.X.; Lu, H.; Sun, G.F.; Wang, Y.K. Study on ultra-light foamed concrete with high volume fly ash. *New Build. Mater.* **2013**, *40*, 74–76+79.
26. Chen, L.Y.; Yang, A.; Hong, F.; Ma, Y.; Wang, J.; Qiao, H. Influence of different fly ash content on the performance and pore size of foamed concrete. *Concrete* **2021**, 137–140.
27. Zheng, N.N.; He, Z.; Sun, H.Y.; Wang, K.; Tong, M.D. Research on the Foamed Concrete with High Volume Fly Ash. *J. Wuhan Univ. Technol.* **2009**, *31*, 96–99+119.